Influence of the phosphoric acid-doping level in a polybenzimidazole membrane on the cell performance of high-temperature proton exchange membrane fuel cells

Yuka Oono[a], Atsuo Sounai[b], Michio Hori[a,*]

[a] Fuel Cell Research Center, Daido Institute of Technology, 10-3 Takiharu-cho, Minami-ku, Nagoya, Aichi 457-8530, Japan
[b] Department of Materials Science & Engineering, Suzuka National College of Technology, Shirako-cho, Suzuka, Mie 510-0294, Japan

ARTICLE INFO

ABSTRACT

The acid migration in phosphoric acid-doped polybenzimidazole (PBI) membrane high-temperature proton exchange membrane fuel cells (HT-PEMFC) during operation is experimentally evaluated to clarify the influence of the acid balance between the membrane and electrodes on cell performance. A method for controlling the amount of phosphoric acid doped in PBI membranes is investigated, and PBI membranes with various amounts of phosphoric acid are prepared. Cell operation tests and AC impedance spectroscopy of cells fabricated with these membranes are conducted. It was found that the amount of phosphoric acid doped in the membranes can be controlled by changing the solution temperature and the immersion time in phosphoric acid solution. It was also found that the HT-PEMFC performance can be improved by optimizing the amount of phosphoric acid doped in the membrane and by diffusion of phosphoric acid into the catalyst layer during the initial stage of cell operation.

© 2008 Elsevier B.V. All rights reserved.

1. Introduction

Residential co-generation systems using low-temperature proton exchange membrane fuel cells (LT-PEMFC) have entered the pre-commercial trial stage in Japan under the program of the New Energy and Industrial Technology Development Organization (NEDO) [1–6]. Under this program, Sanyo Electric Corp., Toshiba Fuel Cell Power System Corp., Matsushita Electric Industrial Corp., Ebara Ballard Corp. and Aishin Seiki Corp. have been examining the possibility of commercializing a 1 kW-class PEMFC residential system based on perfluorinated sulfonic acid membranes that operates in the temperature region 70–80 °C. Such low-temperature operation is an advantage of this type of fuel cell, but it also causes some problems, including low electrical efficiency [2,7] and CO poisoning of the platinum catalyst [8,9]. Furthermore, perfluorinated sulfonic acid polymer electrolytes only exhibit high proton conductivities at high humidities.

High-temperature PEMFCs (HT-PEMFCs) have the potential to solve the problems inherent with LT-PEMFCs. In order to realize such a HT-PEMFC, a number of basic polymers have been investigated for the preparation of acid–base electrolytes, including polybenzimidazole (PBI) [10], polyethylene oxide (PEO) [11], polyvinyl alcohol (PVA) [12,13], polyacrylamide (PAAM) [14,15], and polyethylenimine (PEI) [16].

Many experimental [17–26] and analytical [27–30] studies have been conducted on HT-PEMFCs using a phosphoric acid-doped PBI membrane, which functions most efficiently in the temperature range 120–200 °C [17], and several reports have described the endurance of these membranes [23,31–33]. Furthermore, PBI composites [34–40] have also been developed to improve the performance and/or stability of PBI membranes. HT-PEMFCs do not require large shift converters or selective oxidizers due to their high CO tolerance, which exceeds 10,000 ppm [31,41–43]. Neither do they require humidifiers, because proton transport in the PEM occurs without water dragging [44,45]. They can also be used without vaporizers for supplying steam to a fuel reformer, because the vapor produced by electrode-reaction thermal heat is recirculated. HT-PEMFCs are anticipated to be used for residential applications, because they are cheaper and more efficient than phosphoric acid fuel cells (PAFCs) [46–49]. HT-PEMFCs require cell voltages of over 0.7 V to achieve higher system efficiencies than LT-PEMFCs; however, their cell performance is currently still low compared with such a target. The reason for their low performance is thought to be that oxygen cannot diffuse to the catalyst sites at a sufficiently

* Corresponding author. Tel.: +81 52 612 6111x2508; fax: +81 52 612 5623.
E-mail address: hori@daido-it.ac.jp (M. Hori).

high rate, and the resulting overpotential loss is quite high for the reduction of oxygen at the cathode [20,50].

In order to realize high efficiency HT-PEMFC residential systems, the Daido Institute of Technology (DIT) and Suzuka National College of Technology have been developing PBI/phosphoric acid HT-PEMFCs that can achieve high cell voltages. To reduce the overpotential at the cathode and to achieve a high cell voltage, it has been proposed that phosphoric acid as a proton carrier in the cathode side be reduced, and that instead of using only phosphoric acid, a thin polymer proton carrier, such as the ionomer used for LT-PEMFC, be dispersed in the cathode catalyst. Oxygen should then be diffused at a sufficiently high rate through the thin proton carrier, and the oxygen carrier mechanism should differ from that of the conventional phosphoric acid-doped PBI ionomer, which cannot achieve high performance [51].

As the first stage of this investigation, an attempt was made to clarify the mechanism for the migration of phosphoric acid doped in the PBI membrane from the membrane to the electrodes during cell operation and to clarify how this influences cell performance. Ex situ tests were conducted to ascertain the relationship between the change in doping level with the temperature of the acid solution and the time in which the PBI membranes were immersed during doping. PBI membranes with various phosphoric acid-doping levels were prepared and power generation tests were conducted on cells using membranes with several acid-doping levels. One doping method involves prior doping of the acid in both the membrane and catalyst layers; however, the method adopted in this study was to dope all the phosphoric acid in the membrane, because the authors have more extensive experience with this method [32].

AC impedance spectroscopy was used to clarify the effect of acid-doping level on cell performance. This technique has been used to provide information on the three main processes that limit cell performance: charge transfer, mass transport and ohmic resistance in single cells [52–54], LT-PEMFC stacks [55,56], HT-PEMFCs [17] and PAFCs [57]. The cells were disassembled after the cell operation tests had been completed, and the weights and dimensions of the membranes were measured after removing the electrodes, in order to assess the phosphoric acid migration in the cells.

2. Experimental

2.1. Acid-doping level ex situ test survey

Three PBI membranes with areas of $3\,cm \times 3\,cm$ and thicknesses of approximately $40\,\mu m$ were supplied by a collaborative organization, and their weights and dimensions were measured with a high-precision balance (AUW120D, Shimadzu Corp., Japan) and micrometer, respectively. The three membranes were then immersed in an 85% phosphoric acid solution: one membrane at

20 °C for approximately 500 min, another at 40 °C and the other at 60 °C for 80 min. In order to avoid acid condensation due to evaporation during heating, the phosphoric acid was kept in a covered container in a water bath at the given temperature. The membranes were removed from the container at intervals, the surfaces wiped, and their weights and dimensions measured. In this study, the acid-doping level was defined as the percentage ratio of membrane weight increment from the membrane weight prior to doping to the weight of the acid-containing membrane after doping.

2.2. PBI membrane preparation

PBI membranes with different acid-doping levels of 65%, 71%, 75% and 78% were prepared for single cells and used to evaluate the influence of acid-doping level on cell performance. In order to achieve the target acid-doping levels, PBI membranes with active areas of $5\,cm \times 5\,cm$ and thicknesses of approximately $40\,\mu m$ were immersed in 85% phosphoric acid solution at 20, 40 or 60 °C for times ascertained from the acid-doping level ex situ test survey. Their weights and dimensions were measured before and after doping.

2.3. Electrode preparation

Carbon paper (TGP-H-090, Toray Corp., Japan) was employed as the gas diffusion layer (GDL). For wet proofing, the carbon paper was immersed in a 12 wt.% polytetrafluoroethylene (PTFE; DuPont) dispersion for a few minutes and dried at 80 °C in an atmospheric oven for 15 min. A microporous layer (MPL), which consisted of Ketjenblack carbon (EC-600JD, Akzo Nobel Corp., UK) and PTFE powder (DuPont) as a binder (weight ratio of 65:35), was deposited ($2\,mg\,cm^{-2}$) on the surface of the wet-proofed carbon paper using a dry-deposition facility [58]. The carbon paper with a MPL was sintered at a temperature of 350 °C in an atmospheric furnace for 15 min to melt the PTFE binder, and it was then rolled to flatness [58].

Catalyst ink was prepared by the addition of polyvinylidene fluoride (PVDF; Kureha Corp., Japan) and N-methyl-2-pyrrolidone (NMP; Sigma–Aldrich Corp., USA) to a Pt–Co/C catalyst powder (Pt + Co:C weight ratio of 50:50, TKK Corp., Japan) [23]. After magnetically stirring (PSH-4A, As One Corp., Japan) the catalyst ink for 60 h, it was evenly spread on the MPL-deposited carbon paper using an adjustable doctor blade (MHAI-13, Mitutoyo Corp., Japan). The electrode was dried at a temperature of 80 °C in an atmospheric oven for 1 h and was kept at 160 °C in a vacuum furnace for 25 h to degas the NMP solvent from the electrode. The average thickness of the catalyst layer (CL) was 20 μm and the Pt loading of the electrode was approximately $0.7\,mg\,cm^{-2}$. The same electrode was used for both the anode and cathode. An electron probe microanalyzer
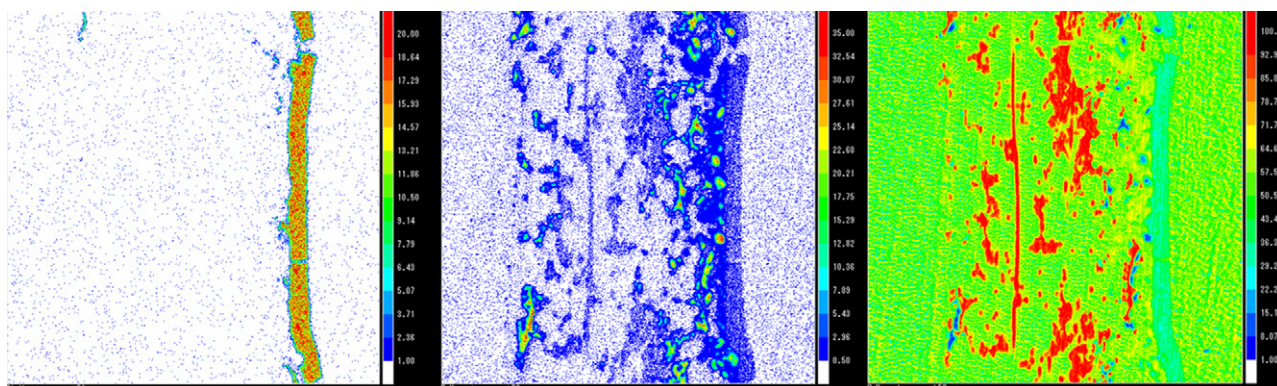

Fig. 1. Typical EPMA cross-sectional images of the electrode composed of a GDL, MPL and CL: (a) platinum, (b) fluorine, and (c) carbon images.
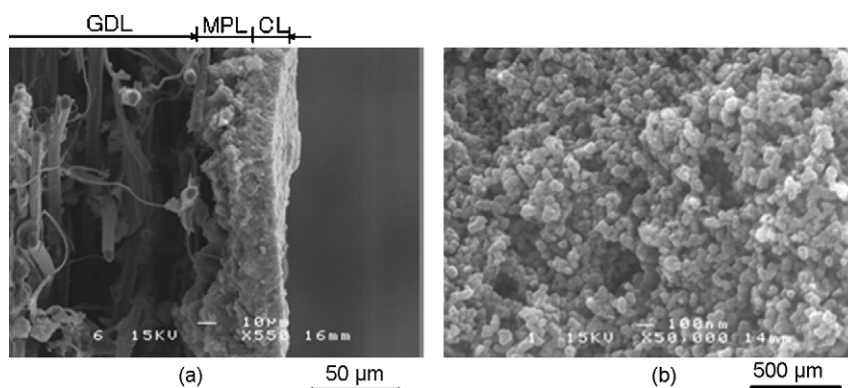
Fig. 2. Typical SEM micrographs of the electrode: (a) cross-sectional micrograph of the electrode composed of a GDL, MPL and CL and (b) surface micrograph of the catalyst layer.

(EPMA; EPMA-1610, Shimadzu, Japan) was employed to observe the cross-section of the electrode consisting of a GDL, a MPL and a CL.

2.4. Single cell assembly

The acid-doped PBI membrane and the electrodes were sandwiched together using a cell holder (JARI, Japan) to form a membrane electrode assembly (MEA). The cell holder was composed of a pair of graphite plates, which functioned as current collectors, and two stainless-steel end plates. The graphite plates have an active area of 25 cm^2 with machined serpentine flow channels. Two end plates with heaters attached and eight screw bolts were used to clamp the MEA together with the graphite plates.

2.5. Single cell test

The single cells were installed in fuel cell test stands (Kofloc Corp., Japan) equipped with reactant mass flow-controllers, an electronic load (Kikusui Electronics Corp., Japan) for controlling the electric current, an AC milliohm tester (Model-3566, Tsuruga Electric Corp., Japan) with a constant frequency of 1 kHz, and a personal computer for equipment monitoring and data output. The cells were operated at 150 °C under a 0.1 MPa atmosphere of pure hydrogen and air without humidification for 450 h. The flow rates of hydrogen and air were 130 mL min^{-1} (stoich: 3.7) and 310 mL min^{-1} (stoich: 3.7), respectively.

A potentiostat–galvanostat (HZ-5000 HAG-3001, Hokuto Denko Corp., Japan) was used for chronocoulometry (CC) measurements of the hydrogen crossover rate through the PBI membrane [59].

During the measurement, single cells were operated at 150 °C with pure hydrogen at the anode and nitrogen at the cathode. Under these operation conditions, a voltage of 0.2 V was applied across the cell, so that hydrogen crossing through the membrane was electrochemically oxidized. During the measurement of the hydrogen crossover rates of the cells, the hydrogen and nitrogen flow rates were controlled at 300 and 500 mL min^{-1}, respectively.

Impedance spectra of single cells were measured at 150 °C by sweeping the frequency range 20,000–0.01 Hz at cell operation times of 0, 50, 100, 150, 250 and 450 h using a frequency response analyzer (FRA 5020A, NF Corp., Japan) connected to a potentiostat–galvanostat (HZ-5000 HAG-3001, Hokuto Denko Corp., Japan) in constant-current mode at a DC current of 5 A (0.2 A cm^{-2}) and an AC amplitude of 0.5 A. The flow rates of hydrogen and air during the measurements were the same as those used for the single cell tests.

2.6. Evaluation of acid migration

After approximately 450 h of cell operation, all the cells were disassembled and both electrodes were scraped away from the membranes. The weights and dimensions of the membranes were then measured. The amount of phosphoric acid exhausted from the cells was evaluated by analyzing the concentration of phosphoric acid in the water exhausted from the cells using inductively coupled plasma mass spectroscopy (ICPMS; ICPM-8500, Shimadzu, Japan). Phosphoric acid migration in the cells was evaluated based on the weights and dimensions of the membranes before and after doping and after cell testing.
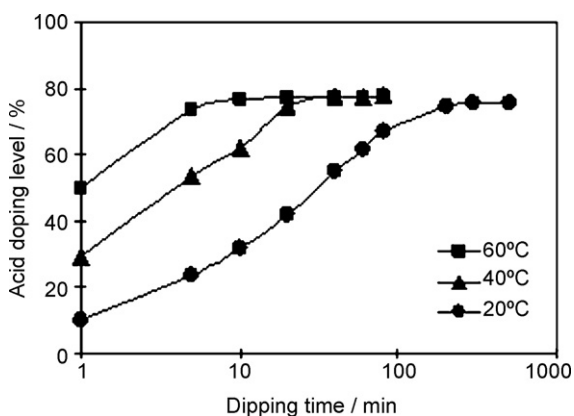

Fig. 3. Influence of phosphoric acid solution temperature and immersion time on the acid-doping level of PBI.
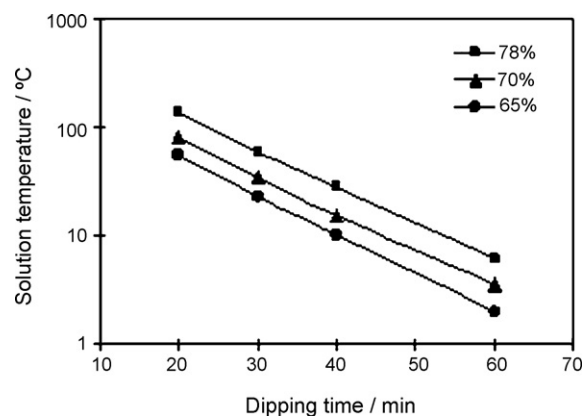

Fig. 4. Relationship between the solution temperature and the immersion time to achieve designated acid-doping levels of 65%, 70% and 78%.
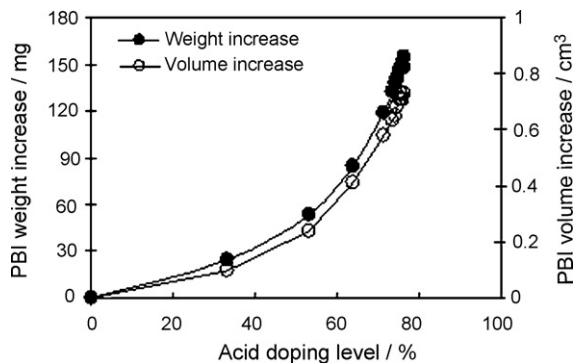
Fig. 5. Relationship between the increase in the weight/volume and acid-doping level of the PBI membrane at 40 °C.

Fig. 7. Relationship of cell voltage, internal resistance at 0.2 A cm^{-2}, and leak current with respect to the acid-doping levels.

3. Results and discussion

3.1. Structural analysis of electrode

Fig. 1 shows typical EPMA cross-sectional images of an electrode composed of a GDL, MPL and CL, observed before assembling the electrodes and membrane in a single cell. The thicknesses of the GDL, MPL and CL are 280, 30 and 20 μm, respectively. Fig. 1(a) and (b) indicates that platinum is limited to the CL, and that fluorine from PTFE is distributed in the GDL and MPL.

Fig. 2(a) shows a cross-sectional SEM micrograph of the electrode indicating that the surface of the GDL is filled with the MPL, and Fig. 2(b) shows the surface of the CL in contact with the membrane. During the initial period of cell operation, phosphoric acid migrates from the PBI membrane, through the interfaces, and into the porous CL shown in Fig. 2(b).

3.2. Ex situ test survey for acid-doping level

For preliminary evaluation of the influence of the acid-doping level of PBI membranes on cell voltage, the acid-doping level was experimentally verified as being controllable. Fig. 3 shows the changes in the acid-doping level with time, obtained by immersing the PBI membranes (areas of 25 cm^2) in acid solutions at 20, 40 and 60 °C. At 60 °C, the acid was rapidly doped into the PBI membrane to the equilibrium level of 78% for an 85% phosphoric acid solution [32] over a period of less than 10 min. On the other hand, at temperatures of 40 and 20 °C, the acid was slowly doped into the PBI membranes up to the same equilibrium level, taking approximately 30 and 300 min, respectively. Thus, higher acid temperatures resulted in a more rapid acid-doping rate. However, irrespective of the solution temperature, the PBI membranes eventually equilibrated at the same acid-doping level of approximately 78%.
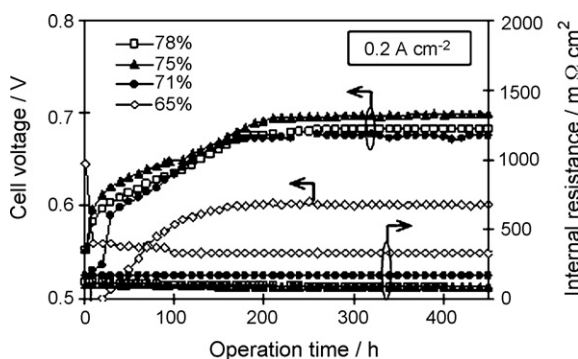
Fig. 4 shows the relationship between the immersion time for acid doping up to levels of 60%, 70%, and 78% and the temperature of the acid solution. There is an inversely proportional relationship between the immersion time up to the designated acid-doping level plotted with a non-logarithmic scale, and the solution temperature plotted with a logarithmic scale. Such a relationship shows that it is possible to control the acid-doping level of the PBI membrane by managing the solution temperature and the immersion time.

Fig. 5 shows the relationship between the increase in the acid-doping weight/volume and the acid-doping level of the PBI membrane with an initial area of 5 cm × 5 cm and initial thickness of 40 μm, at a temperature of 40 °C. The increase in the PBI membrane volume was calculated as the difference between the initial and expanded volume, obtained by taking the product of the experimentally measured length, width and thickness. There is a good correlation between the weight and volume increases and the increase in the acid-doping level; not only does the PBI membrane weight increase, but its volume also increases.

3.3. Single cell test

Fig. 6 shows the cell voltage and internal resistance over time for single cells with acid-doped PBI membranes at levels of 65%, 71%, 75% and 78%, and at 0.2 A cm^{-2}. The internal resistance was measured at a constant frequency of 1 kHz using an AC milliohm tester. All the cell tests were conducted for 450 h (19 days). It was found that all the cell voltages had reached the saturation level after 200 h of operation. The slow increase in cell voltage is thought to be due to the time required for volatilization of the solvent in the PBI membrane and the CL; therefore, the phosphoric acid flows slowly into the pores formed by solvent volatilization, and consequently, the proton conductivity is gradually improved.

Fig. 6. Cell voltage and internal resistance over time for single cells with acid-doping levels of 65%, 71%, 75% and 78% at 0.2 A cm^{-2}.
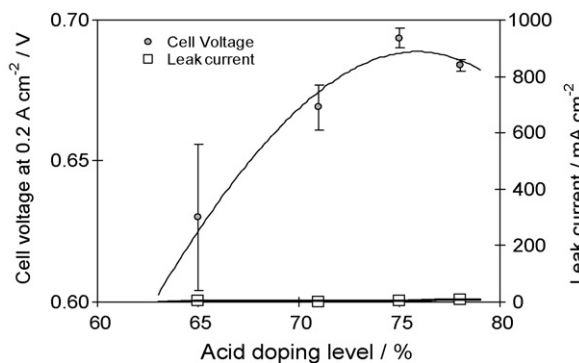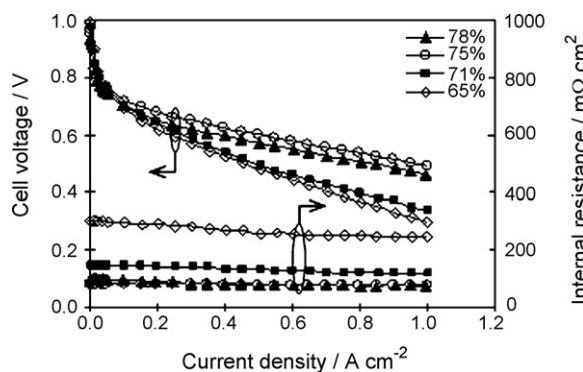

Fig. 8. Influence of the acid-doping levels of PBI membranes on I–V characteristics and internal resistance of single cells.
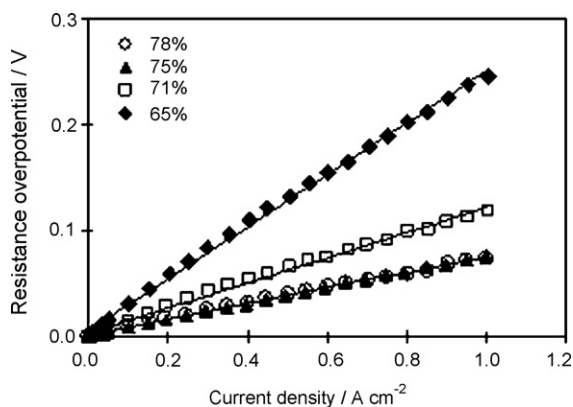
Fig. 9. Relationship of resistance overpotential and current density for single cells with various acid-doping levels.
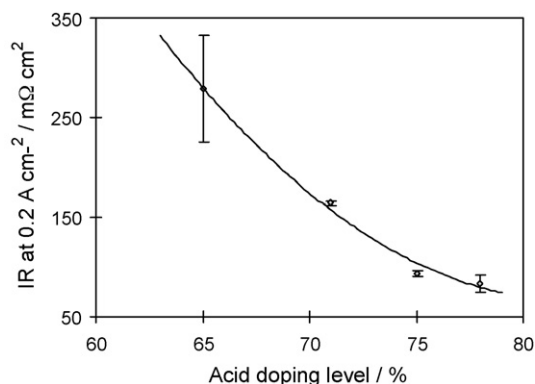

Fig. 10. Relationship of cell internal resistance at $0.2\,A\,cm^{-2}$ and the acid-doping level.

Fig. 7 shows the relationship of the cell voltage and internal resistance to the acid-doping level at an operation time of 450 h. The cell voltage becomes higher with the increase in acid-doping level from 65% to 75%, peaks at around 75%, and then declines slightly with an increase in the acid-doping level over 75%. The relationship between the leak current of each cell obtained from the CC measurements and the doping levels are also shown in Fig. 7. There was negligible crossover detected for all acid-doping levels, which verified that reduction of the acid-doping level in PBI membranes does not cause crossover.

Fig. 8 shows the *I–V* curves and internal resistance for single cells with PBI membranes at acid-doping levels of 65%, 71%, 75% and 78% after 450 h of operation. The stoichiometric flow rates of fuel and oxidant were 1.4 and 5, respectively. For acid-doping levels up to

75%, the cell voltage increases and the cell resistance declines with an increase in the acid-doping levels. With regard to the cell voltage drop from the open circuit voltage to the inflection point of the *I–V* curves in the low current density region below $0.1\,A\,cm^{-2}$, which is often considered as the activation overpotential, there were no significant differences among the single cells with various acid-doping levels. On the other hand, there was significant dependence of the resistance overpotential, which is usually defined as the product of the *I–V* curve slope and the current density, on the acid-doping levels.

In order to clarify this tendency, the relationship between the resistance overpotential of the single cells with various acid-doping levels and the current density is shown in Fig. 9, and the relationship of the internal resistance at $0.2\,A\,cm^{-2}$ with the acid-doping level is shown in Fig. 10. It is thought that such an increase in the cell internal resistance with reduction in the acid-doping level is caused by the reduction in the activation area of the catalyst layers, as shown in Fig. 11. For a single cell with a doping level below 75%, it is thought that there was not enough phosphoric acid migrating from the PBI film to the catalyst layers to obtain a sufficient active area, as shown schematically in Fig. 11(a) and (b). On the contrary, for the single cell with a doping level above 75%, it is thought that the catalyst layers were flooded with phosphoric acid that migrated from the PBI film, as shown in Fig. 11(c).

3.4. AC impedance diagnosis for cell performance

AC impedance was used to clarify the influence of acid-doping level on the three main processes that limit cell performance: charge transfer, mass transport and ohmic resistance. AC impedance spectra of single cells with acid-doping levels of 65%, 71%, 75% and 78% were measured at a current density of $0.2\,A\,cm^{-2}$ throughout their entire operation, including the cell conditioning processes. During the measurement, pure hydrogen and air or oxygen were supplied to the anode and cathode sides, respectively.

Fig. 12 shows typical AC impedance spectra for a cell with an acid-doping level of 75% when air was supplied to the cathode side. Two comparatively distinct arcs and one indistinct arc are observed in the regions of high and low frequency, respectively. With respect to these arcs, previous reports [17,52–57] have indicated that the high frequency intercept of the kinetic loop and the real impedance axis expresses the sum of the ohmic resistance of the membrane, etc. In addition, the distance from the high-frequency real axis intercept to the next lower-frequency real axis intercept represents the anodic and cathodic charge transfer, and the third low frequency arc represents the mass transport impedance that occurs under conditions such as high current density, low airflow or cathode flooding. According to these previous studies, the AC impedance spectra suggest that the ohmic resistance of the membrane, etc., does not change significantly over time, even though there is acid
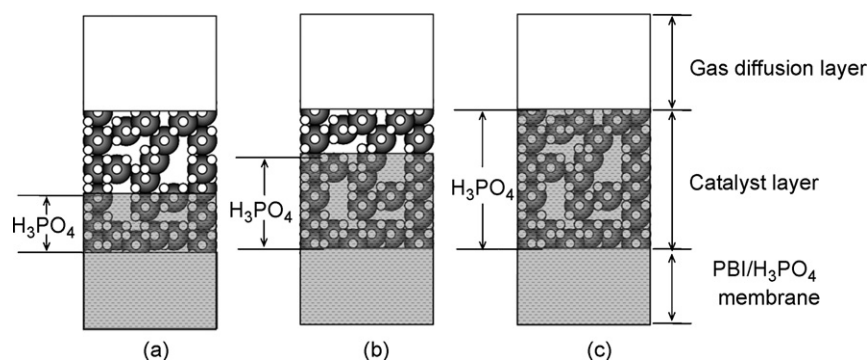

Fig. 11. Schematic diagram illustrating the difference in the amount of phosphoric acid migration from the PBI film to the catalyst layer in single cells with different acid-doping levels of (a) 65%, (b) 71%, and (c) 78%.
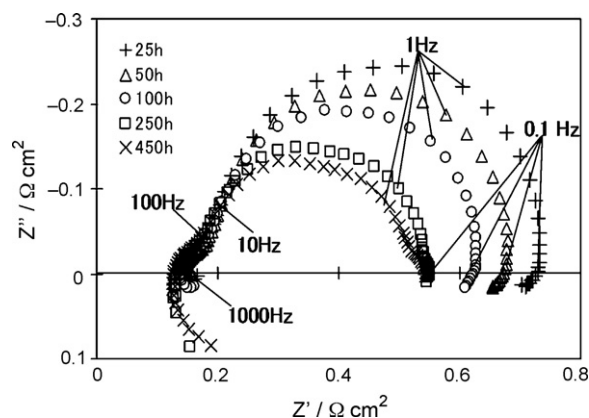
Fig. 12. AC impedance spectra of a single cell with an acid-doping level of 75% at operation times of 25, 50, 100, 250 and 450 h at current density of 0.2 A cm^{-2} with pure hydrogen and air supplied to the anode and cathode sides, respectively.

Fig. 14. Change in the membrane weight before doping, after doping, and after the power generation tests.

migration from the membrane to the catalyst layer. They also imply that the charge transfer decreases over time with the volatilization of the solvent contained in the PBI membrane and catalyst layers and that the third low frequency arc begins from 450 h with flooding of the CL with phosphoric acid that migrated from the membrane.

Fig. 13 shows the impedance spectra of single cells with acid-doping levels of 65%, 71%, 75% and 78% when oxygen is supplied to the cathode side. Two high-frequency arcs and one distorted low-frequency arc are observed. The shapes of these arcs suggest the following that the ohmic resistance of the membrane, etc., decreases with increasing acid-doping level. They also imply that the charge transfer resistance does not necessarily depend on the acid-doping level and that the mass transport resistance of the cathode CL increases with an increase in the acid-doping levels. Therefore, the result shown in Fig. 7, where the cell performance has a maximum around an acid-doping level of 75%, is supported by the AC impedance results; the ohmic resistance decreases and the mass transport resistance increases with increasing acid-doping level, and the sum of both resistances has a minimum value around an acid-doping level of 75%.

3.5. Evaluation of acid migration

In order to have supporting data for the discussions on both the results of the single cell tests in Section 3.3 and the AC impedance spectra in Section 3.4, the weights of the membranes were mea-
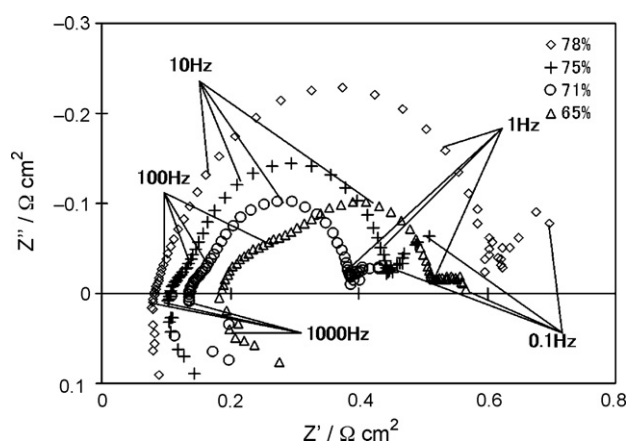
sured before doping, after doping and after cell operation tests. The membrane weights divided by the active area are shown in Fig. 14. Before doping, the four membranes had almost the same weights. With acid-doping, the weights increased to 2.86, 3.48, 3.98 and 4.54 times that of the initial weight for doping levels of 65%, 71%, 75% and 78%, respectively. After the cell operation tests, the weights decreased to 2.03, 2.18, 2.32 and 2.32 times the initial weight, respectively.

In addition to the weight measurements, the concentrations of phosphoric acid included in the total water exhausted from the cells were analyzed using ICPMS after the cell operation tests. Fig. 15 shows typical amounts of phosphoric acid included in the water exhausted from cells with acid-doping levels of 65% and 78% after 450 h operation (1.2×10^{-7} and 2.3×10^{-7} mg cm^{-2}). The results indicate that the amounts of phosphoric acid included in the water exhausted from the cell were negligible, for both low and high acid-doping levels. By combining the results of Figs. 15 and 14, it was estimated that the amounts of phosphoric acid remaining in the catalyst layers after operation of single cells with acid-doping levels of 65%, 71%, 75% and 78% (5.3, 7.9, 10.3 and 12.4 mg cm^{-2}) were 0.83, 1.30 and 1.66 and 2.21 times that of the initial membrane weights, respectively. In the light of this result and those of the single cell tests in Section 3.3 and the AC impedance spectra in Section 3.4, it was concluded that approximately 10 mg cm^{-2} is the optimum

Fig. 13. AC impedance spectra of single cells with acid-doping levels of 65%, 71%, 75%, 78% at an operation time of 450 h at current density of 0.2 A cm^{-2} with hydrogen and oxygen supplied to the anode and cathode sides, respectively.
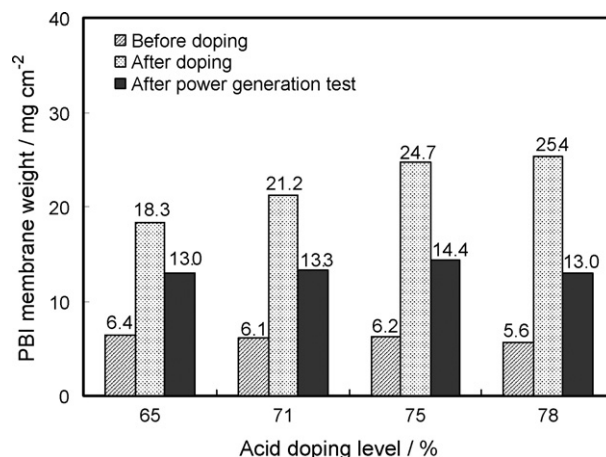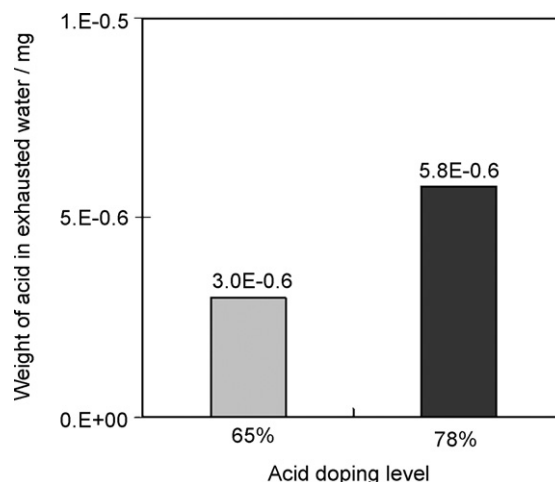

Fig. 15. Weight of phosphoric acid included in the water exhausted from single cells with acid-doping levels of 65% and 78% during cell operation over 450 h.

amount of phosphoric acid in a CL with a thickness of approximately 20 μm, as used in this study.

4. Conclusions

For HT-PEMFCs based on phosphoric acid-doped PBI membranes, it was clarified that the amounts of phosphoric acid doped in the membranes could be controlled by changing the phosphoric acid solution temperature and the immersion time in the phosphoric acid solution. Cell performance was improved by optimizing the amounts of phosphoric acid doped in the membrane and by the diffusion of phosphoric acid into the catalyst layer at the initial stage of cell operation. It was concluded that approximately 10 mg cm^{-2} is the optimum amount of phosphoric acid for a catalyst layer with a thickness of approximately 20 μm.

References

[1] K. Endo, Proceedings of the 4th International Hydrogen & Fuel Cell Expo, Keynote, 2008, p. 27.
[2] T. Omata, J. Fuel Cell Technol. 7 (2) (2007) 6.
[3] M. Hiwatari, J. Fuel Cell Technol. 7 (2) (2007) 11.
[4] H. Yamada, J. Fuel Cell Technol. 7 (2) (2007) 24.
[5] M. Ochi, J. Fuel Cell Technol. 7 (2) (2007) 29.
[6] A. Matsui, M. Kawai, Y. Kimura, H. Tachi, J. Fuel Cell Technol. 7 (2) (2007) 33.
[7] T. Omata, Proceedings of the 4th International Hydrogen & Fuel Cell Expo, FC-2, 2008.
[8] W. Shi, M. Hou, Z. Shao, J. Hu, Z. Hou, P. Ming, B. Yi, J. Power Sources 174 (2007) 164.
[9] C.H. Wan, Q.H. Zhuang, Electrochim. Acta 52 (2007) 4111.
[10] B. Xing, O. Savadogo, Electrochem. Commun. 2 (2000) 697.
[11] P. Donoso, W. Gorecki, C. Berthier, F. Defendini, C. Poinsignon, M. Armand, Solid State Ionics 28–30 (1988) 969.
[12] S.P. Weeks, J.J. Zupancic, J.R. Swedo, Solid State Ionics 31 (1988) 117.
[13] M.A. Vargas, R.A. Vargas, B.E. Mellander, Electrochim. Acta 44 (1999) 4227.
[14] J.C. Lassègues, B. Desbat, O. Trinquet, F. Cruege, C. Poinsignon, Solid State Ionics 35 (1989) 17.
[15] D. Rogriguez, C. Jegat, O. Trinquet, J. Grondin, J.C. Lassègues, Solid State Ionics 61 (1993) 195.
[16] M.F. Daniel, B. Desbat, F. Cruege, O. Trinquet, J.C. Lassègues, Solid State Ionics 28–30 (1988) 637.
[17] J. Zhang, Y. Tang, C. Song, J. Zhang, J. Power Sources 172 (2007) 163.
[18] I.M. Petrushina, V.A. Bandur, N.J. Bjerrum, F. Cappeln, L. Qingfeng, J. Electrochem. Soc. 149 (2002) D143.
[19] J. Lobato, M.A. Rodrigo, J.J. Linares, K. Scott, J. Power Sources 157 (2006) 284.
[20] N.H. Jalani, M. Ramani, K. Ohlsson, S. Buelte, G. Pacifico, R. Pollard, R. Staudt, R. Datta, J. Power Sources 160 (2006 1096).
[21] Z. Qi, S. Buelte, J. Power Sources 161 (2006) 1126.
[22] A.R. Korsgaard, R. Refshauge, M.P. Nielsen, M. Bang, S.K. Kaer, J. Power Sources 162 (2006) 239.
[23] Y. Zhai, H. Zhang, G. Liu, J. Hu, B. Yi, J. Electrochem. Soc. 154 (2007) B72.
[24] C. Pan, Q. Li, J.O. Jensen, R. He, L.N. Cleemann, M.S. Nilsson, N.J. Bjerrum, Q. Zeng, J. Power Sources 172 (2007) 278.
[25] J.R.P. Jayakody, S.H. Chung, L. Durantino, H. Zhang, L. Xiao, B.C. Benicewicz, S.G. Greenbaum, J. Electrochem. Soc. 154 (2) (2007) B242.
[26] K.C. Neyerlin, A. Singh, D. Chu, J. Power Sources 176 (2008) 112.
[27] D. Cheddie, N. Munroe, J. Power Sources 156 (2006) 414.
[28] D.F. Cheddie, N.D.H. Munroe, J. Power Sources 160 (2006) 215.
[29] J. Peng, S.J. Lee, J. Power Sources 162 (2006) 1182.
[30] J. Peng, J.Y. Shin, T.W. Song, J. Power Sources 179 (2008) 220.
[31] J. Baurmeister, T. Kohno, Proceeding of FCDIC Symposium, vol. 13, 2006, p. 122.
[32] A. Sounai, K. Sakai, Proceeding of FCDIC Symposium, vol. 13, 2006, p. 125.
[33] A. Sounai, J. Baurmeister, T.J. Schmidt, J. Fuel Cell Technol. 7 (2) (2007) 86.
[34] P. Staiti, M. Minutoli, S. Hocevar, J. Power Sources 90 (2000) 231.
[35] C. Hasiotis, L. Qingfeng, V. Deimede, J.K. Kallitsis, C.G. Kontoyannis, N.J. Bjerrum, J. Electrochem. Soc. 148 (5) (2001) A513.
[36] M.Y. Jang, Y. Yamazaki, J. Power Sources 139 (2005) 2.
[37] A. Carollo, E. Quartarone, C. Tomasi, P. Mustarelli, F. Belotti, A. Magistris, F. Maestroni, M. Parachini, L. Garlaschelli, P.P. Righetti, J. Power Sources 160 (2006) 175.
[38] S.W. Chuang, S.L.C. Hsu, C.L. Hsu, J. Power Sources 168 (2007) 172.
[39] Y. Zhai, H. Zhang, Y. Zhang, D. Xing, J. Power Sources 169 (2007) 259.
[40] T.H. Kim, T.W. Lim, J.–C. Lee, J. Power Sources 172 (2007) 172.
[41] P. Krishnan, J.S. Park, C.S. Kim, J. Power Sources 159 (2006) 817.
[42] H. Xu, Y. Song, H.R. Kunz, J.M. Fenton, J. Power Sources 159 (2006) 979.
[43] C.P. Wang, H.S. Chu, Y.Y. Yan, K.L. Hsueh, J. Power Sources 170 (2007) 235.
[44] Y.L. Ma, J.S. Wainright, M.H. Litt, R.F. Savinell, J. Electrochem. Soc. 151 (2004) A–8.
[45] Q. Li, R. He, R.W. Berg, H.A. Hjuler, N. Bjerrum, Solid State Ionics 168 (2004) 177.
[46] A.J. Appleby, J. Power Sources 58 (1996) 153.
[47] Y. Watanabe, M. Matsumoto, K. Takasu, J. Power Sources 61 (1996) 53.
[48] H.Y. Kwak, H.S. Lee, J.Y. Jung, J.S. Jeon, D.R. Park, Fuel (Guildford) 83 (2004 2087).
[49] A. Sounai, J. Baurmeister, T.J. Schmidt, M. Hori, J. Fuel Cell Technol. 7 (2) (2007) 76.
[50] Z. Liu, J.S. Wainright, M.H. Litt, R.F. Savinell, Electrochim. Acta 51 (2006) 3914.
[51] J.H. Kim, H.J. Kim, T.H. Lim, H.I. Lee, J. Power Sources 170 (2007) 275.
[52] O. Antoine, Y. Bultel, R. Durand, J. Electroanal. Chem. 499 (2001) 85.
[53] I.A. Schneider, H. Kuhn, A. Wokaun, G.G. Schere, J. Electrochem. Soc. 152 (10) (2005) A2092.
[54] X. Yuan, H. Wang, J.C. Sun, J. Zhang, Int. J. Hydrogen Energy 32 (2007) 4365.
[55] X. Yuan, J.C. Sun, M. Blanco, H. Wang, J. Zhang, D.P. Wilkinson, J. Power Sources 161 (2006) 920.
[56] X. Yuan, J.C. Sun, H. Wang, J. Zhang, J. Power Sources 161 (2006) 929.
[57] R.H. Song, D.J. Kim, C.S. Kim, D.R. Shin, J. New Mater. Electrochem. Syst. 4 (2001) 47.
[58] J. Yu, Y. Yoshikawa, T. Matsuura, M.N. Islam, M. Hori, Electrochem. Solid-State Lett. 8 (3) (2005) A152.
[59] J. Yu, T. Matsuura, Y. Yoshikawa, M.N. Islam, M. Hori, Electrochem. Solid-State Lett. 8 (3) (2005) A156.